Effect of pre-treatment and calcination temperature on Al_2O_3-ZrO_2 supported Ni-Co catalysts for dry reforming of methane

Ahmed Sadeq Al Fatesh[a]*, Jehad K. Abu-Dahrieh[b*], Hanan Atia[c] , Udo Armbruster[c], Ahmed A. Ibrahim[a] , Wasim U. Khan[a], Ahmed Elhag Abasaeed[a,] Anis H. Fakeeha[a]

[a] Chemical Engineering Department, College of Engineering, King Saud University, P.O. Box 800, Riyadh 11421, Saudi Arabia.

[b] School of Chemistry and Chemical Engineering, Queen's University Belfast, Belfast BT9 5AG, Northern Ireland, UK.

[c] Leibniz Institute for Catalysis, Albert-Einstein-Str. 29A, 18059, Rostock, Germany.

Corresponding author: Ahmed. Sadeq Al Fatesh, Jehad K. Abu-Dahrieh

Email: aalfatesh@ksu.edu.sa[1],j.abudahrieh@qub.ac.uk[2]

Abstract

In this paper, the effect of pre-treatment and calcination temperature on a series of 5%Co/Al_2O_3-ZrO_2, 5%Ni/Al_2O_3-ZrO_2 and 2.5%Co-2.5%Ni/Al_2O_3-ZrO_2 catalysts for dry reforming of methane was investigated. Main focus of our research was to improve the catalyst stability by proper pre-treatment and reaction conditions. The first approach aimed at the catalyst pre-treatment by using bimetallic systems and the second strategy at the *in situ* suppression of coke. The catalytic activity of bimetallic system was indeed higher compared to the monometallic in the temperature range of 500-800 °C (space velocity 18000 $ml \cdot h^{-1} \cdot g_{cat}^{-1}$, CH_4/CO_2 = 1). The bimetallic catalyst calcined at 800 °C showed highest CH_4 conversion without deactivation and gave a H_2/CO ratio of 91% and 0.96, respectively, and good stability with less coke deposition over 28 h at 800 °C reaction temperature. This improvement is assigned to the synergism between Co and Ni, their high dispersion according to interaction with support. It has been shown in our work that pretreatment temperatures and atmospheres have strong impact on stability of the catalyst. TEM, XRD and TPO investigations confirmed that the slight catalyst deactivation was related to the formation of multiwall carbon nanotubes with hollow inner tube structure. The addition of small amounts of steam or oxygen during DRM improved both the catalyst activity and stability as the bimetallic catalyst lost around 9.4% conversion in DRM, 5.4% in presence of water and only 3.2% in presence of O_2.

Keywords: Bimetallic catalyst, Dry reforming, Methane, Stability, Deactivation, Regeneration

Introduction

In recent years industrial processes have been established to convert methane into syngas (H_2, CO). Some of these industrial processes comprise steam reforming and partial oxidation while lab-scale studies are also in progress on dry reforming of methane (DRM) and/or a combination of above mentioned processes [1]. The respective equations (Eqs. 1-3) are stated below. Dry reforming of methane would be attractive as it simultaneously converts main greenhouse gases CH_4 and CO_2 [2-7]. The produced syngas can be directly used for reactions like hydroformylation or the H_2/CO ratio can be adjusted for Fischer–Tropsch, dimethyl ether and methanol processes, which require higher H_2/CO ratios. DRM is usually associated with the reverse water–gas shift reaction Eq. (4).

$CH_4 + H_2O \rightarrow 3H_2 + CO$	$\Delta H° = 206$ kJ/mol	Steam reforming	(1)
$CH_4 + \frac{1}{2}O_2 \rightarrow 2H_2 + CO$	$\Delta H° = -38$ kJ/mol	Partial oxidation	(2)
$CH_4 + CO_2 \rightarrow 2H_2 + 2CO$	$\Delta H° = 247$ kJ/mol	Dry reforming	(3)
$CO_2 + H_2 \rightarrow CO + H_2O$	$\Delta H° = 37.6$ kJ/mol	reverse water-gas shift	(4)

Noble metals display superior performance in this reaction but are generally too expensive [8]. Various emerging catalyst technologies for different applications were also recently reported in the literature [9-17]. Transition metals, for instance Ni and Co, are universally considered as suited catalysts for DRM due to their low costs. On the other hand, they were still not commercialized for DRM because they are prone to rapid deactivation as a consequence of carbon deposition. The following reactions are considered as the main source of coke formation in dry reforming of methane:

$CH_4 \rightarrow 2H_2 + C$	ΔH°= 75 kJ/mol	Methane decomposition	(5)
$2CO \rightarrow CO_2 + C$	ΔH°= -172 kJ/mol	Boudouard reaction	(6)

Both these reactions are limited by thermodynamic equilibrium. At high temperature, Boduouard reaction (Eq. 6) is not significant for coke formation, while methane decomposition (Eq. 5) is favoured.

To tackle the issue of carbon formation, several researchers investigated in depth the nature of the constituents of the catalysts and the operating conditions in order to improve their activity and stability in the process. This was done by supporting the active metals on materials such as alumina [18-22] which has advantages including low cost, great mechanical strength and high surface area. However, the phase transformations and interaction with metals during temperature variation affect and limit its applicability [20]. To solve this issue, alumina can be mixed with other supports to promote the catalyst activity and in general mixed oxide catalysts have better catalytic properties than pure oxides [23-27]. For instance, Bellido et al. [27] tested the effect of mixing ZrO_2 and CaO on the activity of nickel-based catalyst in DRM. They found that the electrical properties, such as particle conductivity as a function of anionic vacancies of the support, have a proportional influence on catalytic activity. The other two approaches to avoid carbon deposition during the reforming of hydrocarbons are to use a high oxygen mobility support or to add basic oxide such as ZrO_2 to stabilize the alumina, which facilitates gasification of the carbon simultaneously [5]. Also, Perez-Camacho et al. [5] studied the effect of adding different high oxygen mobility dopants such as CeO_2, ZrO_2, or yttrium-stabilised zirconia

(YSZ) on a Ni perovskite catalyst ($Na_{0.5}La_{0.5}Ni_{0.3}Al_{0.7}O_{2.5}$). They found that the perovskite doped with 80.9% ZrO_2 and 15.2% CeO_2 gave the lowest amount of carbon deposits.

The pre-treatment conditions of the catalysts play a significant role for the final performance. It has been reported that the activity of supported metal catalysts strongly depends on the thermal treatment (either *ex situ* or *in situ*) before reaction, i.e., calcination and reduction temperatures [28, 29]. Calcination temperature has a substantial effect on dispersion of the active metal particles and the metal-support interaction and therefore influences the rate of carbon formation on the catalyst surface [30]. Wang and Ruckenstein [31] tested the effect of calcination temperature on Co-supported catalysts and found that degree of catalyst reduction and structural properties varied with calcination temperatures, which then altered the catalytic performance. Similarly, the investigation by Sun et al. [32] emphasized the significance of calcination temperature for the development of surface textural properties and phase structure. Our group [33] investigated the effect of combining Ni and Co metal catalysts and found that the interaction of Ni and Co gave less carbon formation with higher activity. The importance of calcination temperature on Ni/γ-Al_2O_3 catalysts was also studied [28] as well as the effect of reduction temperature on the catalysts using hydrogen. Calcination temperature enhanced the activity while the reduction temperature increased basicity and therefore increased the CO_2 adsorption. The enhancement of CO_2 adsorption provided more oxygen species on the surface of the catalysts, which increase the gasification of the formed carbon (Eq. 6, back reaction) and prevent carbon deposition.

This paper presents the catalytic performance of a series of Co, Ni and Ni-Co-based catalysts supported on Al_2O_3-ZrO_2. The effect of calcination temperature and of different

catalyst reduction protocols will be discussed. Moreover, the long-term stability of the bimetallic catalyst was examined, and the best-performing catalyst was also tested in presence of small amounts of steam or oxygen to study the impact of feed composition on stability.

Experimental

Materials

The chemicals used include cobalt acetate tetrahydrate [$(CH_3COO)_2Co$], nickel acetate tetrahydrate [$(CH_3COO)_2Ni$], zirconium butoxide/butylate [$(OC_4H_9)_4Zr$] solution (80 wt.% in 1-butanol) and aluminium sec-butoxide/butylate [$(C_{12}H_{27}O_3)Al$] and all were of analytical grade. These chemicals were supplied by Aldrich, UK and Merck.

Catalyst preparation

In order to get the crystal water-free salts, all the metal precursors were oven dried at 100 °C for 24 h. The weight loss was similar to the water content and therefore no decomposition took place. Prior to use, the salts were ground and sieved below 100 μm in order to dissolve and react easily with Al-butylate. These salts were the source for cobalt and nickel. 48 g of Zr-butylate and 25 g of Al-sec-butoxide were mixed in a 250 ml three-neck round-bottom glass flask equipped with a reflux cooler and magnetic stirrer. The mixture was subjected to heating under stirring up to 130 °C followed by addition of 2.59 g of the dried cobalt acetate. After keeping the mixture under magnetic stirring for 2 h at 130 °C, the contents in the round-bottom flask were transferred into a 500 ml beaker containing 75 g of iso-propanol. The residues (butylates) from round-bottom flask were

poured into another beaker containing 75 g of iso-propanol. Finally, clear solutions with slightly pink and green colour were obtained for cobalt and nickel, respectively. These solutions were subjected to reflux for 1 h after addition of 27 g of distilled water within 1 min under intensive stirring. In order to avoid loss of iso-propanol, a water-containing round-bottom flask was used to cover the beaker. Finally, a glass frit was used to separate precipitate from the liquid after cooling the solution down to room temperature. No washing was necessary. Based on this recipe, three precursors were prepared with 5 wt% Ni, 5 wt% Co and 2.5 wt% Ni + 2.5 wt% Co on the ZrO_2-Al_2O_3 support. With each of these precursors, four different pre-treatment protocols were applied (groups 1-4, Table 1). After drying the as-prepared precursor overnight at room temperature, part of the solid was reduced *in situ* in the DRM reactor with H_2 at 800 °C without preceding calcination (group 1). Another part also was not calcined but reduced *ex situ* with H_2 at 800 °C, transferred to the reactor and reduced *in situ* with H_2 at 800 °C (group 2). A third part of the sample was heated with 2K/min and calcined *ex situ* under air at 550 °C for 6 h, transferred to the reactor and reduced with H_2 at 800 °C (group 3). The last part was heated with 2 K/min and calcined *ex situ* at 800 °C for 6 h and subsequently reduced in the reactor with H_2 at 800 °C (group 4). The catalysts were named after the active metals and the respective pre-treatment group (Table 1).

Table 1: Overview on pre-treatment protocols and catalyst names. All samples were dried at ambient conditions overnight before pre-treatment

Group	Pre-treatment	Catalyst	Name
1	- not calcined - reduced in situ (H_2 flow, 800 °C, 1.5 h)	5%Co/ZrO_2-Al_2O_3	Co-1
		5%Ni/ ZrO_2-Al_2O_3	Ni-1
		2.5%Co+2.5%Ni/ ZrO_2-Al_2O_3	CoNi-1
2	- not calcined - reduced ex situ (H_2 flow, 800 °C)	5%Co/ ZrO_2-Al_2O_3	Co-2
		5%Ni/ ZrO_2-Al_2O_3	Ni-2

	- reduced in situ (H_2 flow, 800 °C, 1.5 h)	2.5%Co+2.5%Ni/ ZrO_2-Al_2O_3	CoNi-2
3	- calcined (air flow, 550 °C, 6 h) - reduced in situ (H_2 flow, 800 °C, 1.5 h)	5%Co/ ZrO_2-Al_2O_3	Co-3
		5%Ni/ ZrO_2-Al_2O_3	Ni-3
		2.5%Co+2.5%Ni/ ZrO_2-Al_2O_3	CoNi-3
4	- calcined (air flow, 800 °C, 6 h) - reduced in situ (H_2 flow, 800 °C, 1.5 h)	5%Co/ ZrO_2-Al_2O_3	Co-4
		5%Ni/ ZrO_2-Al_2O_3	Ni-4
		2.5%Co+2.5%Ni/ ZrO_2-Al_2O_3	CoNi-4

Characterization of catalyst

Micromeritics Tristar II 3020 surface area and porosity analyser was used to evaluate the Brunauer–Emmett–Teller (BET) specific surface area of the catalysts prior to reaction. 0.2 g of each sample was used for every analysis. Prior to analysis, moisture and other adsorbed gases on the catalysts surface were removed by degassing the samples at 250 °C for 3 h. Barrett-Joyner-Halenda (BJH) method was adopted to determine the pore size distribution using the corresponding nitrogen adsorption-desorption isotherm.

Temperature-programmed reduction using hydrogen (H_2-TPR) and oxidation (O_2-TPO) experiments were carried out using Micromeritics AutoChem II apparatus. For each analysis, 70 mg of the sample were pre-treated with Argon (30 ml/min) for H_2-TPR and with Helium (30 ml/min) for O_2-TPO at 150 °C for 30 min. The samples were cooled to ambient temperature before starting the analysis. For H_2-TPR, the sample temperature was raised from ambient to 1000 °C in an automatic furnace under atmospheric pressure. During temperature ramping, H_2/Ar mixture with a volume ratio 10/90 was flowing at 40 ml/min while heating rate was kept constant at 10 K/min. In O_2-TPO, used for determining the nature of carbon deposits on the spent catalysts, a mixture of O_2 and He was flowing at 30 ml/min at same rate as in H_2-TPR. The outlet gases were monitored by a thermal conductivity detector (TCD) to analyse the hydrogen and oxygen consumption with respect

to temperature in H_2-TPR and O_2-TPO respectively. The amount of carbon deposited during reaction was quantified using Shimadzu thermo-gravimetric analyser. Each spent catalyst with 10-15 mg was subjected to thermal treatment under air from 35 to 1000 °C (ramp rate of 20 K/min) and carbon contents were calculated.

The crystallinity of catalysts before and after reaction was measured by X-ray powder diffraction (XRD). STADI P automated transmission diffractometer (STOE, Darmstadt) equipped with Ge monochromator and CuKα1 radiation was used. The patterns were recorded by a STOE position sensitive detector in the 2θ range of 5 to 70°. The step widths of 0.5 and 100 s per step were used. Flat plates were used to prepared samples.

The morphology of nano-structured carbon deposited over the catalyst surface was analysed by JEOL JEM-1400 transmission electron microscope (TEM). TEM images were recorded at 120 kV accelerating voltage. Prior to analysis, ultrasonic dispersion of catalyst samples was carried out in ethanol at room temperature. A few drops of the suspension containing catalyst sample were placed on a carbon-coated copper grid. The copper grid was then used for imaging for each sample. The actual amounts of each metal, i.e., Co, Ni, Zr and Al were determined using inductively coupled plasma atomic emission spectroscopy (ICP-AES). The results are shown in Table (2).

Table 2: ICP-AES of the prepared catalyst

Sample name	Elements	Theoretical value %	ICP values %
5% Co/Zr-Al	Zr	52	48.6
	Al	15	14.2
	Co	5	4.5
2.5%Co+2.5%Ni/Zr-Al	Zr	52	44.8
	Al	15	13.6
	Co	2.5	2.8
	Ni	2.5	2.6
5%Ni/Zr-Al	Zr	52	45.6

	Al	15	13.1
	Ni	5	4.4

Catalyst activity

As-synthesized catalysts (each 0.15 g) were tested in a fixed-bed microactivity reactor at atmospheric pressure. The reactor was made up of stainless steel and had an I.D. of 9.4 mm and was 30 cm long. A thermocouple was placed in the core of catalyst bed to monitor the reaction temperature. Prior to the DRM test, the metal oxides were reduced to metals with hydrogen (40 ml/min) at 800 °C for 90 min followed by nitrogen purging to remove any residual hydrogen in the reactor. Then the reactor temperature was lowered under flowing nitrogen to set point temperature of 700 °C. The feed gas contained methane and carbon dioxide (17 ml/min each) and nitrogen (11 ml/min) was added as inert. The gas hourly space velocity (GHSV) was 18000 $ml \cdot h^{-1} \cdot g_{cat}^{-1}$ corresponding to a catalyst weight of 0.15 g and a feed flow rate of 45 ml/min. Reaction temperatures ranged from 500 to 800 °C. Shimadzu 2014 gas chromatograph (GC) was used to analyse gases on-line from the reactor outlet using a thermal conductivity detector (TCD). The GC was equipped with two columns, i.e., Molecular Sieve 5A and Porapak Q for product analysis.

Results and Discussion

Catalyst characterization

The XRD patterns for the fresh catalysts are shown in Figure 1a for group 2 (uncalcined + reduced *ex situ*) and group 4 (calcined at 800 °C + reduced *in situ*), respectively. All the catalysts were treated *in situ* at least once at 800 °C and have similar patterns in which all the reflections appeared except the one at 45.2° which only appeared for group 2 catalysts. This reflection can be assigned to metallic Co or Ni according to JCPDS 01-089-7093 and

JCPDS 03-065-0380 references, respectively. This explains the role of calcination in the dispersion and distribution of the active metal on the support surface.

In group 2, Co and Ni do not interact with the support and so small reflexes appeared which could stem from Ni, Co and/or Co-Ni alloy, while in group 4 – covering the samples that were calcined at 800 °C – Co and Ni are strongly interacting with the support and so no Co and Ni reflexes were observed. The reflections at 2θ = 35.6, 50.9 and 60.5 are assigned to ZrO_2 [34] while the signal at 2θ = 30.5° is ascribed to $Al_{0.52}Zr_{0.48}O_{1.74}$ according to JCPDS 00-053-0294. Essential changes were observed in the phase composition when the calcination temperature was set to 800 °C in group 4, as the reflexes of ZrO_2 turned to be more intense due to the formation of tetragonal ZrO_2 [35]. Moreover, the intensity of the reflexes of $Al_{0.52}Zr_{0.48}O_{1.74}$ phase increased due to the calcination at 800 °C. Figure 1b shows XRD patterns of the spent catalysts after 6 h on stream at 700 °C, illustrating graphite peaks in the spent catalysts as it is confirmed by TEM as well. These reflexes appear at 26º for CoNi-2, Ni-2, CoNi-4 and Co-4 and at 43º for CoNi-4 and Co-4. Moreover, the peak intensities for spent CoNi-2 and Ni-2 catalysts are relatively lower than for the fresh materials, indicating the higher dispersion (lower crystallite size) of the bimetallic sample, which can affect their reducibility as will be discussed later. The same behaviour was also found by others [36, 37].

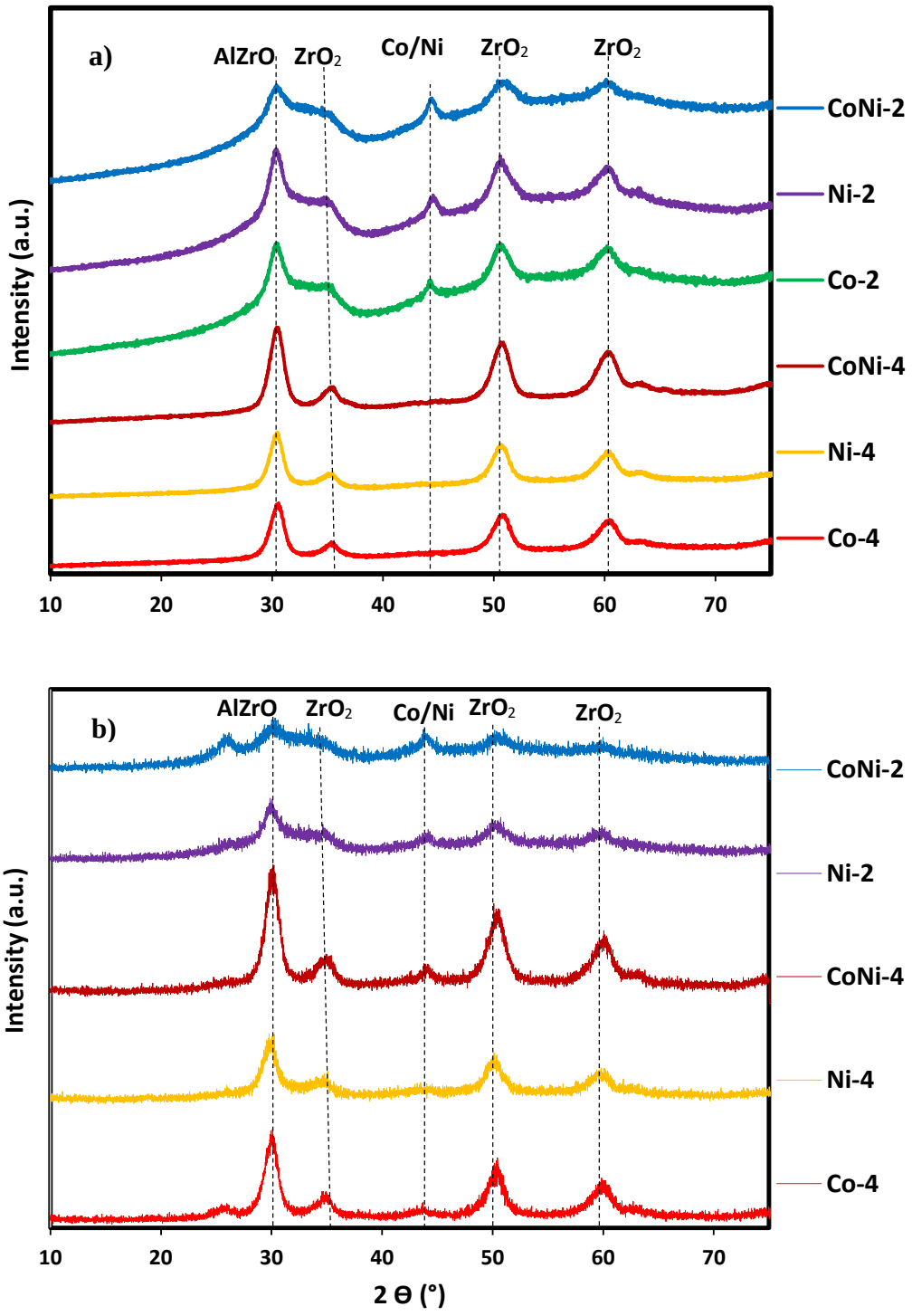

Figure (1): XRD patterns of a) fresh catalysts and b) spent catalysts after 6 h on stream at 700 °C, atmospheric pressure, CH_4: CO_2 =1: 1 in the feed gas. Catalyst weight: 150 mg, WHSV: 18000 ml g^{-1} h^{-1}.

The diffraction pattern of the spent CoNi-4 catalyst after 28 h on stream at 800 °C is shown in Figure 2. The new reflection at 2θ = 26.1° indicates the formation of graphite [38,39], whereas the reflexes at 2θ = 43, 44.5, 53, 62 and 77° can be assigned to graphite carbon [40].

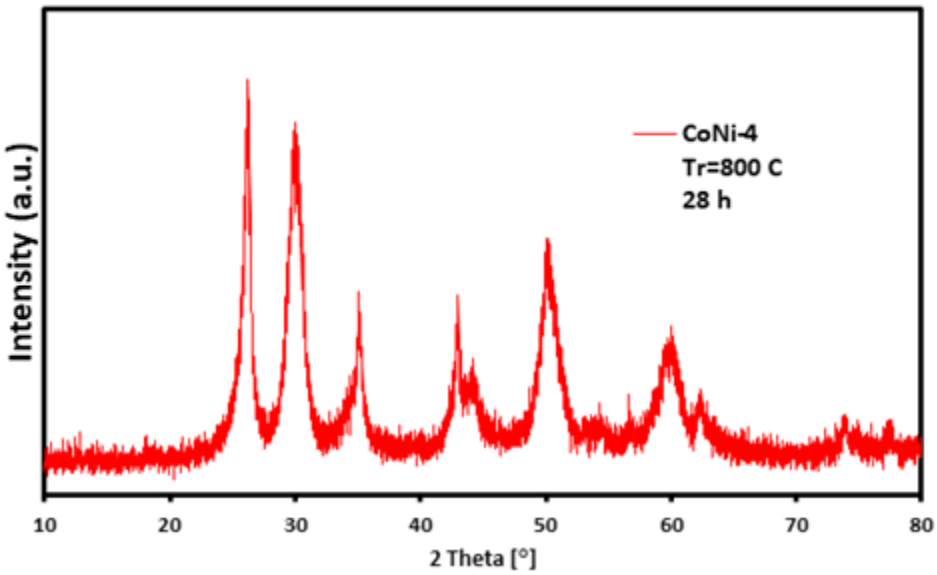

Fig. 2: XRD patterns of spent CoNi-4 catalyst after 28 h on stream at 800 °C, atmospheric pressure, CH_4/CO_2 = 1:1. Catalyst was reduced in H_2 at 800 °C, catalyst weight = 150 mg, WHSV = 18000 $ml \cdot g^{-1} \cdot h^{-1}$.

Figures 3-6 display the nitrogen volumes adsorbed with relative pressure for all the catalysts. All the isotherms are categorized as type II, with hysteresis loop similar to H3 according to IUPAC [41], thus indicating the presence of macropores. Group 1 samples before calcination and/or reduction showed the highest surface area of 384-460 m^2/g. The surface area of groups 2, 3, and 4 were in the range of 15-175, 211-216 and 104.7-129.4 m^2/g, respectively. The effect of calcination temperature can be clearly seen on comparing group 3 and 4. As expected, increasing the calcination temperature of group 4 materials to 800 °C lead to a decrease in the surface area by 43-50%. This means that high calcination temperature triggers sintering and reduction of surface area and thus particle growth. The

effect of pretreatment atmosphere can be elucidated by comparing groups 2 and 4. The loss in surface area of group 4 in comparison with group 2 samples was not as high as compared with group 3 (32%). Calcination temperature has a much higher impact on the surface area compared to the nature of pre-treatment atmosphere. Furthermore, the higher surface area found for group 2 materials could be an explanation for the low crystallinity compared to group 4 as confirmed by XRD.

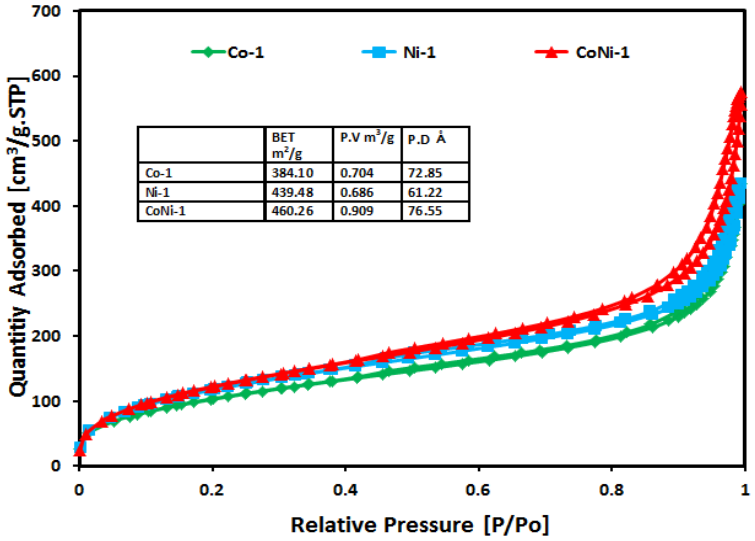

Fig. 3: Adsorption/desorption isotherms, BET pore volumes and pore diameters of group 1 catalysts.

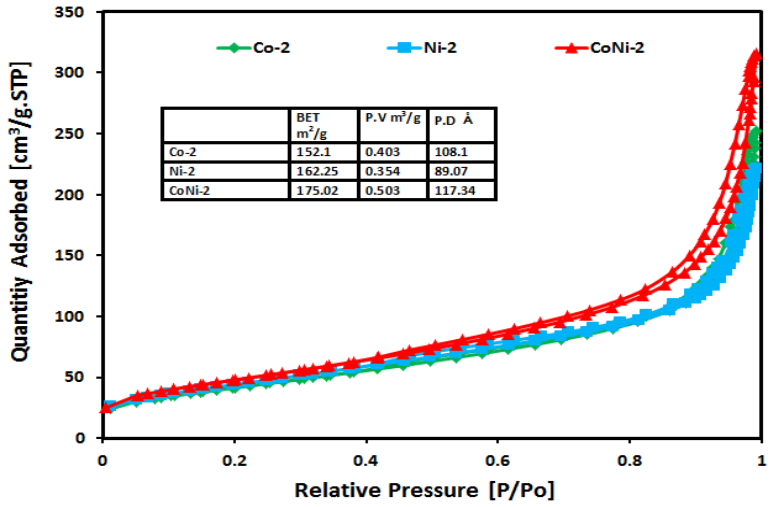

	BET m^2/g	P.V m^3/g	P.D Å
Co-2	152.1	0.403	108.1
Ni-2	162.25	0.354	89.07
CoNi-2	175.02	0.503	117.34

Fig. 4: Adsorption/desorption isotherms, BET pore volumes and pore diameters of group 2 catalysts.

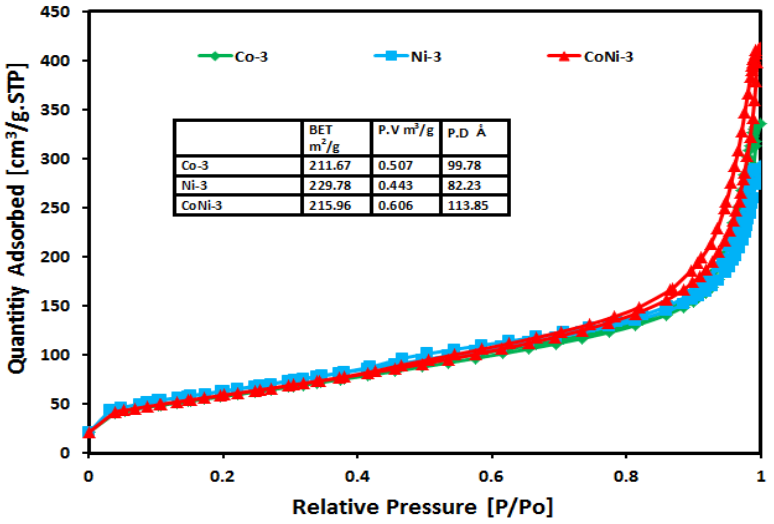

	BET m^2/g	P.V m^3/g	P.D Å
Co-3	211.67	0.507	99.78
Ni-3	229.78	0.443	82.23
CoNi-3	215.96	0.606	113.85

Fig. 5: Adsorption/desorption isotherms, BET pore volumes and pore diameters of group 3 catalysts.

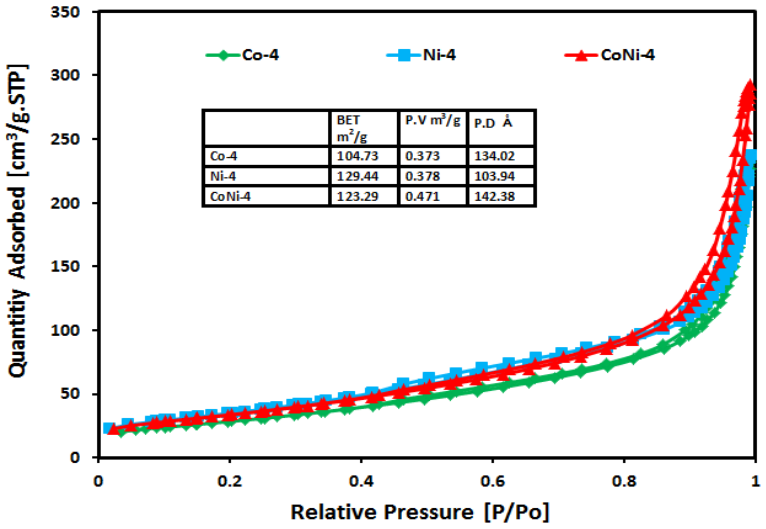

Fig. 6: Adsorption/desorption isotherms, BET pore volumes and pore diameters of group 4 catalysts.

TPR analysis was carried out to determine the catalyst reducibility in respect to the metal-support interaction. Figures 7-9 summarize the TPR plots of the prepared catalysts, which show only one main reduction peak for each catalyst. Nickel-based catalysts have the lowest reduction temperature as Ni is much easier to reduce than Co. The high reduction peak temperature for Co-3 and Co-4 catalysts is attributed to the strong interaction between Co and support. For Co-2 the reduction is different from Co-3 and 4. It possesses a peak near 350 °C which could be assigned to the transition from Co^{3+} to Co^{2+}, and another shoulder around 470 °C can be attributed to the reduction of Co^{2+} to Co^{0} [42]. Another small peak at 550 °C which is present in both Co-2 and Ni-2 is due to metal support interaction. The peak of Ni-based catalysts is attributed to the reduction of bulk NiO to Ni^{0}. Moreover, in all the prepared catalysts, addition of Ni to Co shifts the reduction peak to lower temperature. Low reduction temperature of the bimetallic catalyst is due to the high dispersion as it has been proved by XRD [37]. Setting the calcination temperature to 550 °C (group 3) and to 800 °C (group 4) shifts reduction temperatures to higher values,

indicating strong metal-support interaction (Figures 8 and 9) [44, 45]. For instance, the reduction peaks for bimetallic CoNi-2 (not calcined), CoNi-3 (calcined at 550 °C) and CoNi-4 (calcined at 800 °C) occur at 300, 600 and 770 °C, respectively. The peaks for Ni-4, CoNi-4 and Co-4 catalysts are centred at 720, 760 and 920 °C, respectively.

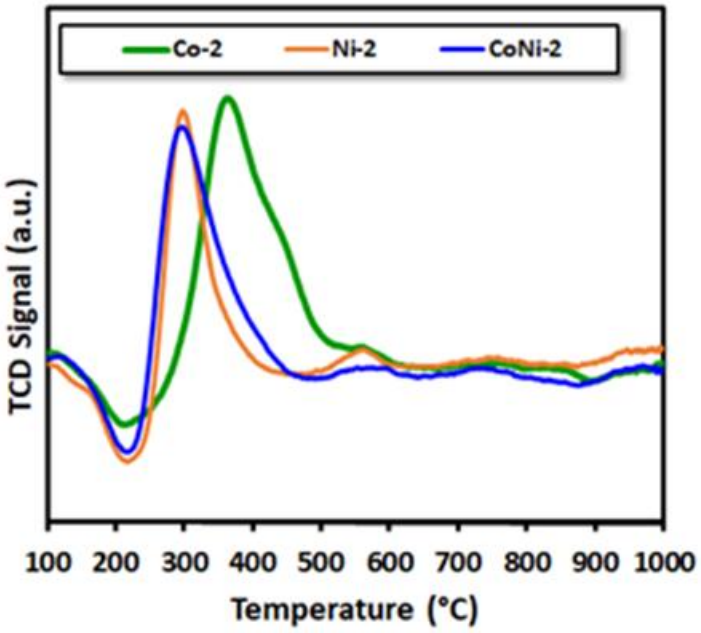

Fig. 7: TPR plots for group 2 catalysts after *ex situ* reduction at 800 °C.

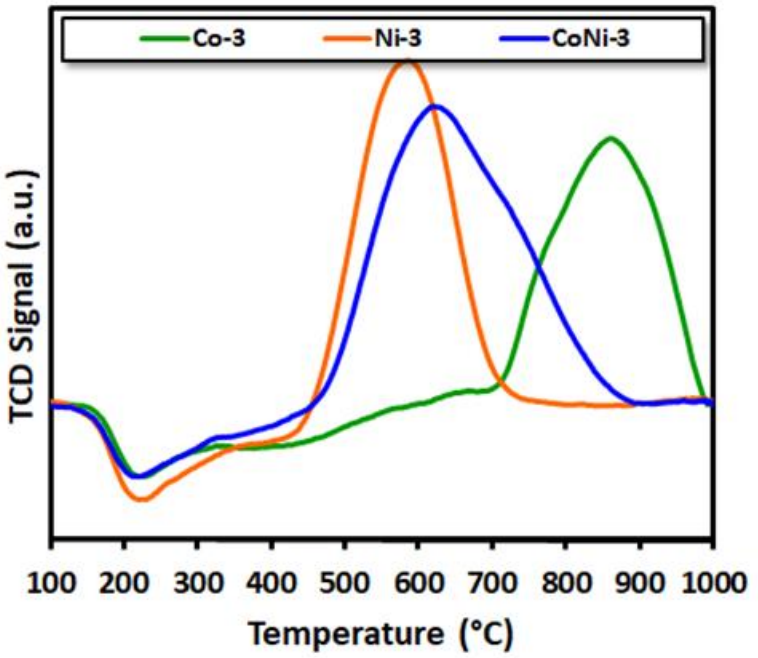

Fig. 8: TPR plots for group 3 catalysts *ex situ* calcined at 550 °C.

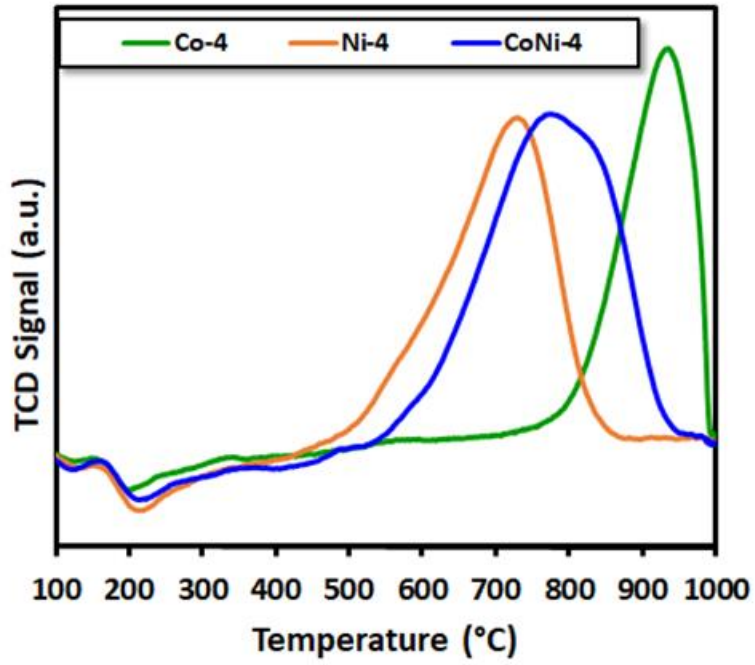

Fig. 9: TPR plots for group 4 catalysts *ex situ* calcined at 800 °C.

Table 3 shows the amount of carbon deposits on the surface of the spent catalysts after 6 h on stream at 700 °C. The carbon deposition on the bimetallic (CoNi-1 and CoNi-2) catalysts is higher than that on the monometallic catalysts.

Table 3: Catalyst activity and amount of carbon deposits from TGA analysis

Group	Catalyst	Conv. CH_4 (%)		Conv. CO_2 (%)		Avg. H_2/CO[c]	D.F.[d] (%)	Carbon TGA[e]
		Initial[a]	Final[b]	Initial[a]	Final[b]			
1	Co-1	38.2	36.8	58.2	53.0	0.67	3.66	1.65
	Ni-1	48.1	47.6	64.5	60.6	0.78	1.04	1.59
	CoNi-1	56.6	53.5	71.3	66.3	0.82	5.50	3.97
2	Co-2	49.5	36.9	63.7	52.5	0.69	25.40	3.15
	Ni-2	67.6	63.0	74.2	69.8	0.80	6.80	6.27
	CoNi-2	71.4	68.1	77.5	75.8	0.93	4.62	19.36
3	Co-3	44.1	45.2	65.1	60.2	0.74	-2.5	1.12
	Ni-3	55.5	58.7	74.5	66.6	0.86	-5.8	3.51
	CoNi-3	51.4	51.0	65.2	64.0	0.79	0.78	1.95
4	Co-4	56.8	57.4	72.1	68.5	0.86	-1.1	19.75
	Ni-4	64.9	64.4	77.4	72.0	0.92	0.77	5.13
	CoNi-4	68.5	67.3	77.4	76.3	0.91	1.80	13.21

Reaction condition: 700 °C, $CH_4 + CO_2$ = 34 ml/min, N_2 = 11 ml/min, catalyst wt. = 0.3 g

[a] 20 min on stream.

[b] Final on stream (360 min).

[c] Average data during time-on-stream.

[d] Deactivation Factor (D.F) = (final CH_4 conversion - initial conversion CH_4)/(initial conversion of CH_4)×100.

[e] Carbon deposition obtained by TGA method (mg).

Figures 10 and 11 show the TGA profiles for the spent catalysts (CoNi-2 and CoNi-4, respectively) after 6 h on stream at 500, 600, 700 and 800 °C. The reaction temperature has a strong effect on the amount of carbon deposited. Both catalysts CoNi-2 and CoNi-4 have the lowest amount of coke deposited after operation at 800 °C.

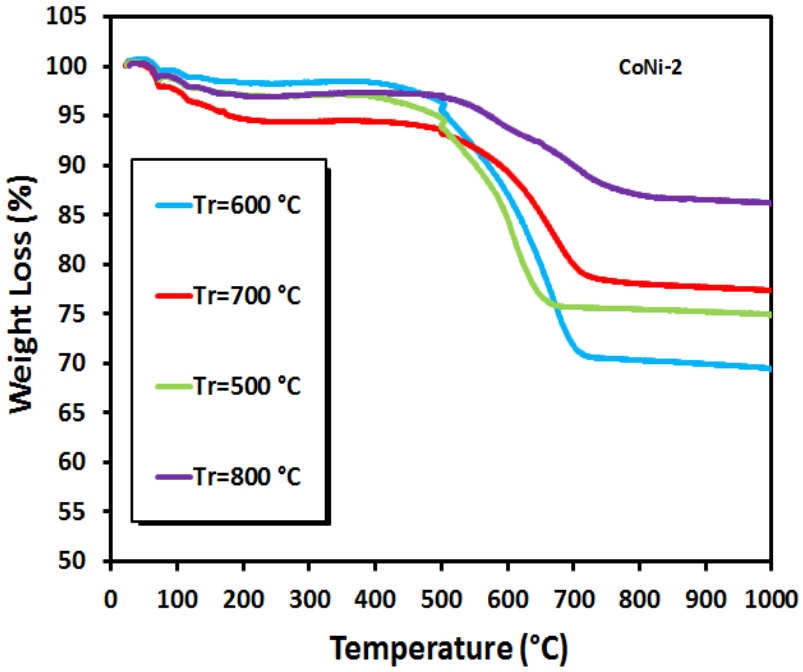

Fig. 10: TGA curves for spent CoNi-2 catalysts from runs at different reaction temperatures, measured in air with heating rate 20 K/min.

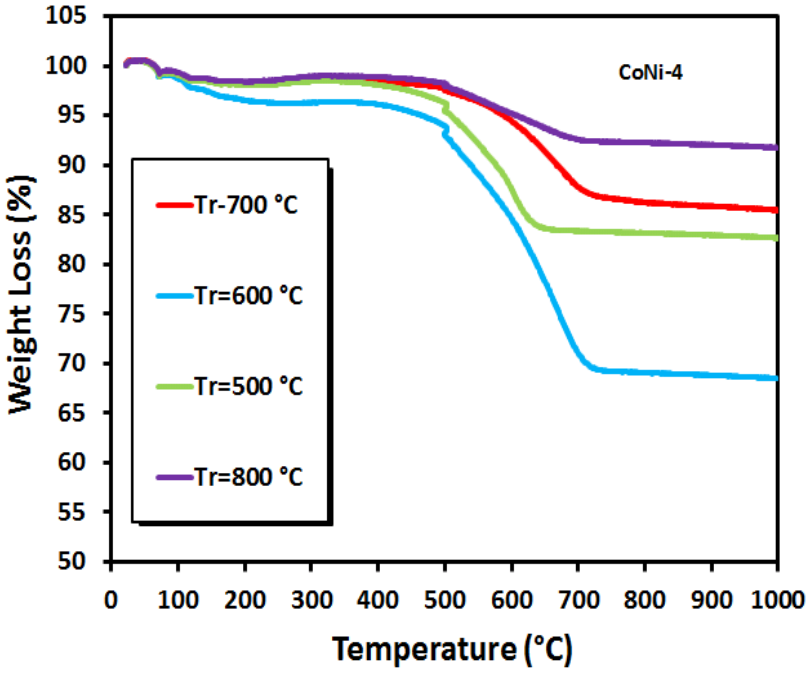

Fig. 11: TGA curves for spent CoNi-4 catalysts from runs at different reaction temperatures, measured in air with heating rate of 20 K/min.

The TEM analysis of the spent CoNi-4 catalyst after reaction for 28 h at 800 °C is shown in Figure 12. The images evidence the formation of multiwall carbon nanotubes of different size together with amorphous carbon. Both ends of the nanotubes were open as seen in Figure 12 a-c. Figure 12 d shows a carbon nanotube with multiple graphitic layers around the hollow inner tube [38, 39].

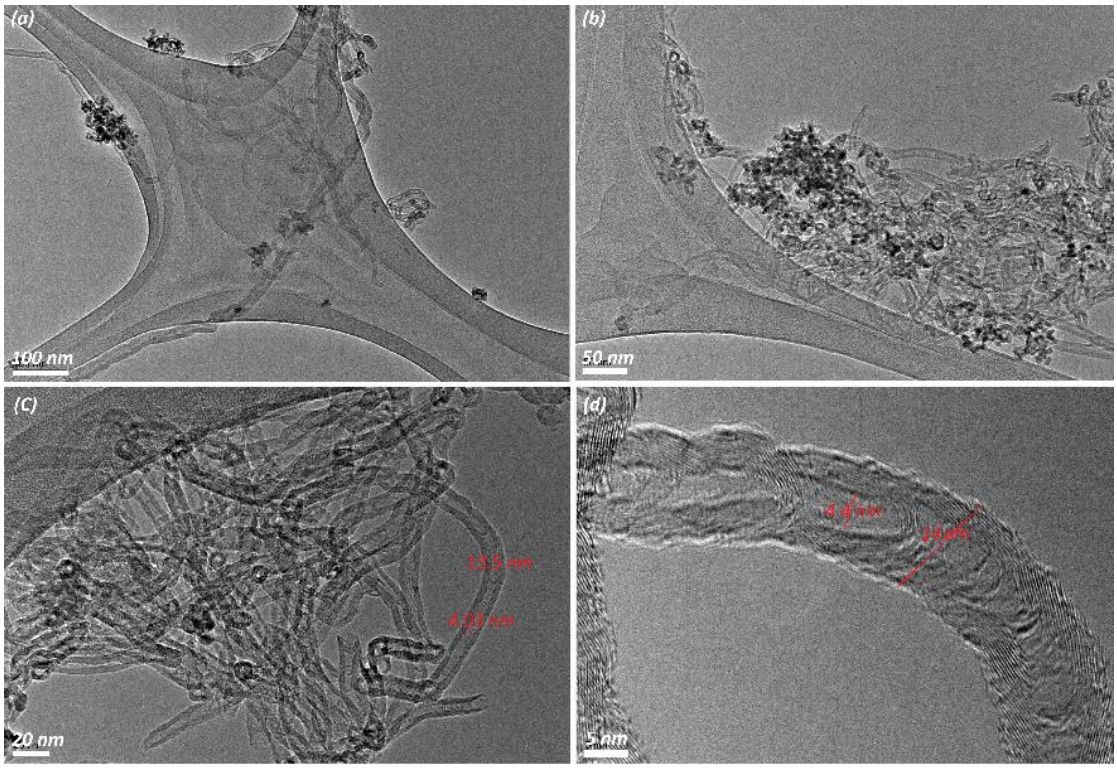

Fig. 12: TEM analysis of the spent CoNi-4 catalyst after reaction for 28 h at 800 °C, atmospheric pressure, CH_4/CO_2 = 1:1. Catalyst was reduced in H_2 at 800 °C, catalyst weight = 150 mg, WHSV = 18000 $ml \cdot g^{-1} \cdot h^{-1}$.

Results from TPO study of the nature of carbon deposited on spent CoNi-4 catalysts after 28 h on stream at 800 °C and after 6 h on stream at 700 °C is shown in Figure 13. The TPO profile for CoNi-4 after 28 h showed one shoulder at 620 °C and another at higher temperature at 720 °C, while the sample after 6 h on stream shows one peak at 600 °C. This carbonaceous matter can be assigned to multiwall carbon nanotubes (low temperature) and graphite (high temperature).

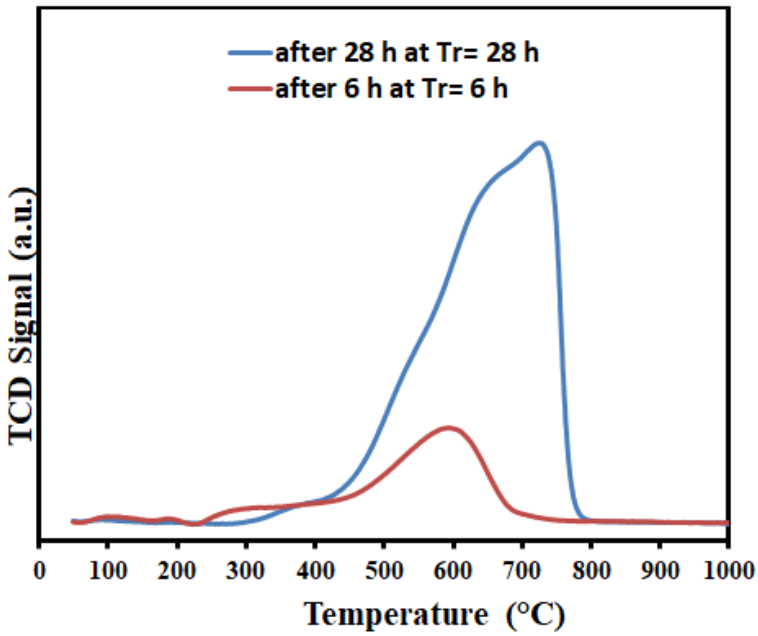

Fig. 13: TPO plots of the spent CoNi-4 catalyst after 28 h on stream at 800 °C and after 6 h on stream at 700 °C.

Catalyst Activity

Table 3 displays the CO_2 and CH_4 conversions and H_2/CO ratios in DRM at 700 °C for all catalysts. The CH_4 conversions were always lower than the corresponding CO_2 conversions and H_2/CO ratios were always less than unity in all groups. This phenomenon can be explained by the occurrence of reversed water-gas shift reaction (RWGS, Eq. 2) in which CO_2 and H_2 are consumed to produce CO and H_2O [43].

The table reveals that in all groups the monometallic nickel-based catalyst gives higher CO_2 and CH_4 conversion than monometallic cobalt-based catalysts. Similar results were found by Gonzalez-de la Cruz [44]. Also, the bimetallic catalysts provide higher CO_2 and CH_4 conversions than monometallic catalysts. The higher activity of these catalysts can be attributed to the synergistic effect between the Co and Ni metals [40]. Gonzalez-de la Cruz et al. [44] investigated the synergistic effect of Zr-supported bimetallic Ni-Co systems on

the DRM activity with *in-situ* X-ray absorption spectroscopy (XAS) and found that even though the monometallic cobalt system is inactive, the Ni–Co bimetallic systems have much higher activity and selectivity in DRM as both metals obviously protect each other from oxidation under reaction conditions. CH_4 conversions of 49.5, 67.6 and 71.4% were observed for Co-2, Ni-2 and CoNi-2 catalysts, respectively. This can be explained by the physical–chemical modification between Co and Ni (low crystallinity (XRD) and low reduction temperature (TPR)) which has an impact on their activity and stability. The higher the activity of the bimetallic catalysts, the higher the carbon deposition (Table 3). The catalysts CoNi-1, CoNi-2, CoNi-3 and CoNi-4 reached CH_4 conversions of 56.6, 71.4, 51.1 and 68.5% and the analysed carbon amounted to 3.97, 19.36, 1.95 and 13.21 mg, respectively. For the least active samples Co-1, Co-2, Co-3 and Co-4 the carbon deposits were measured as 1.65, 3.15, 1.12 and 19.75 mg, respectively. The highest amount of carbon deposition found by sample CoNi-2 could be due to low interaction with the support as it was found by XRD which revealed only small reflexes for Co, Ni or Co-Ni spinel. The carbon deposition can be attributed to both methane decomposition (Eq. 3) and Boudouard reaction (Eq. 4) [46]. Although the carbon deposition on the bimetallic catalysts is high, these catalysts show comparatively high stability in all four groups. This can be attributed to the large pore diameters that are beneficial for the long-term stability as complete pore plugging is hindered. Generally, one reason for the catalyst deactivation could be the carbon deposition within the pores of the catalyst [47, 48]. The initial conversions of CH_4 in the catalysts of groups 4 and 3 are almost the same as the final conversions. However, both groups 1 and 3 showed deactivation and a loss of 5% in CH_4 conversion (deactivation factors of -1.1, 0.77 and 2.5 % for Co-4, Ni-4 and CoNi-4,

respectively). This indicates that the catalyst pre-treatment has a significant effect on the textural properties and on catalytic activity and stability [28]. To get more information on the nature of carbon deposited on the CoNi-4 catalyst surface after 6 h on stream at 700 °C, TEM images were recorded. As shown in Figure 12, multiwall carbon nanotubes were formed with different diameter and orientation and with high degree of disorder which confirms the contribution of reverse Boudouard reaction (Eq. 4) in which CO_2 reacts with any type of deposited carbon [49]. This is in agreement with TPO results. The variation in reaction temperature has been studied over CoNi-2 and CoNi-4. Figures 14 and 15 show the effect of reaction temperature on CO_2 and CH_4 conversion and H_2/CO ratio. Again, CO_2 conversions are higher than the corresponding CH_4 conversions at all reaction temperatures due to RWGS which consumes CO_2 as well. Furthermore, these catalysts showed high stability at all reaction temperatures. This can be explained by the synergistic effect between the metals by forming smaller sized bimetallic oxides that are resistant to be oxidised under the reaction conditions. These two bimetallic catalysts (CoNi-2 and CoNi-4) also have the highest pore diameters. The CH_4 conversions for CoNi-4 are 15, 35, 69 and 90% at 500, 600, 700 and 800 °C, respectively, with the H_2/CO ratio approaching unity at 800 °C. The increase in H_2/CO ratio at high temperature can be explained by an increase of endothermic methane decomposition to carbon and hydrogen.

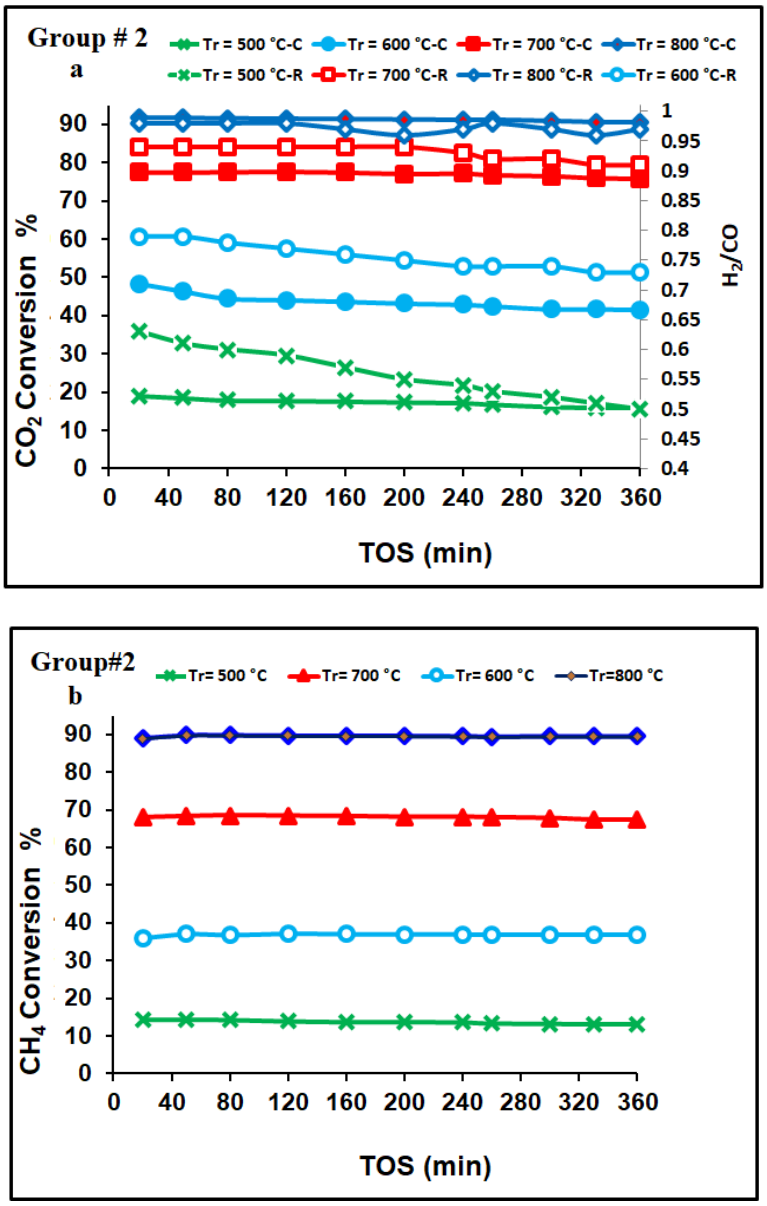

Fig. 14: course of a) CO_2 conversion and H_2/CO ratio and b) CH_4 conversion with time on stream over CoNi-2 at reaction temperatures of 500-800 °C, atmospheric pressure, CH_4/CO_2 = 1:1, catalyst weight = 150 mg, WHSV = 18000 $ml \cdot g^{-1} \cdot h^{-1}$.

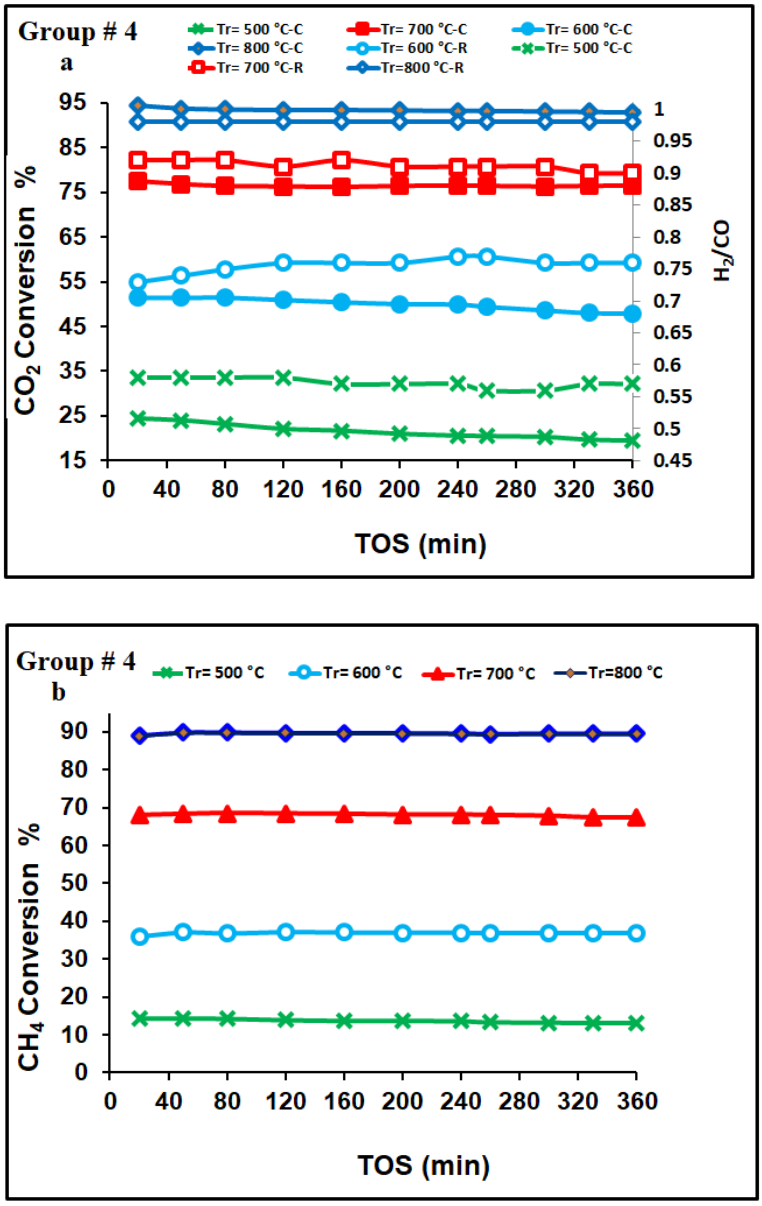

Fig. 15: course of a) CO_2 conversion and H_2/CO ratio and b) CH_4 conversion with time on stream over CoNi-4 at reaction temperature of 500-800 °C, atmospheric pressure, CH_4/CO_2 = 1:1. Catalyst was reduced in H_2 at 800 °C, catalyst weight = 150 mg, WHSV = 18000 $ml \cdot g^{-1} \cdot h^{-1}$.

To distinguish the nature of coke deposits formed at different reaction temperature, a TGA study for spent catalysts after 6 h on stream was conducted (Figures 10 and 11). Coke deposition over CoNi-4 was less than for CoNi-2 at all reaction temperatures, as Co and Ni were better dispersed on the surface of the support due to the strong interaction as it has

been confirmed by TPR. In addition, it possesses the highest pore diameter due to high-temperature pre-treatment of the catalyst [28, 29]. For CoNi-4 (Figure 11), the weight losses are 5, 13, 15 and 30% at 800, 700, 500 and 600 °C, respectively.

Moreover, for both catalysts CoNi-2 (Figure 10) and CoNi-4 (Figure 11) the lowest coke deposition rate was observed at 800 °C. This can be attributed to the fact that the Boudouard reaction (Eq. 4) is exothermic and becomes thermodynamically less favourable above 700 °C [45, 37, 50]. Moreover, at 800 °C the presence of zirconia in the support suppresses the methane decomposition (Eq. 3) and also promotes the reverse Boudouard reaction [5]. The highest amounts of coke deposits were measured at 600 °C, as this intermediate temperature allows both methane decomposition (Eq. 3) and Boudouard reaction (Eq. 4) in remarkable extent [45].

Regarding the activity, CoNi-4 showed high CH_4 conversion of 91% without deactivation and a H_2/CO ratio of 0.96 at 800 °C and therefore it was chosen for further long-term tests (28 h on stream at 800 °C), and the courses of H_2/CO ratio, CO_2 and CH_4 conversion are presented in Figure 16. The catalyst showed only minor loss of its activity after 24 h. However, with ongoing test, sharp drops in CH_4 and CO_2 conversion from 88.8 % to 84 % and from 94 % to 80 %, respectively, were observed (relative loss of initial activity: 5% in CH_4, 15% in CO_2). The main cause of deactivation is carbon deposition as confirmed by TEM (Figure 12), TPO (Figure 13) and XRD (Figure 2) studies with the spent catalyst.

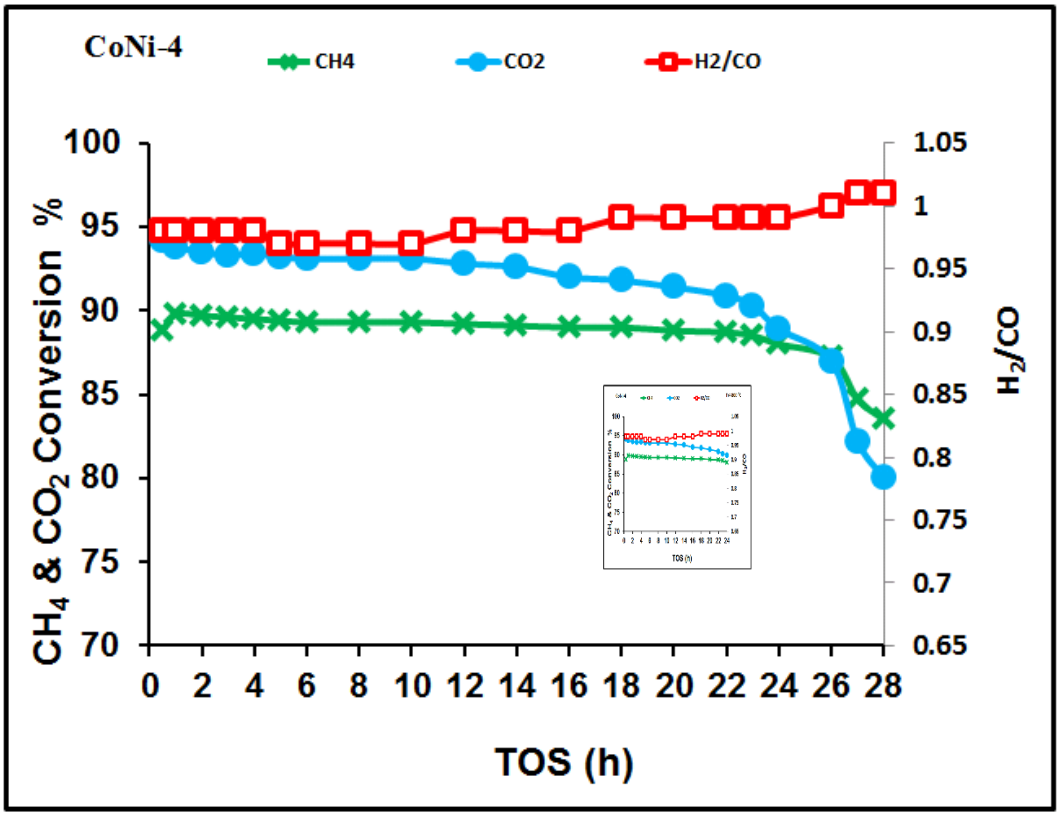
CoNi-4
CH4
CO2
H2/CO
100
95
90
85
80
75
70
1.05
1
0.95
0.9
0.85
0.8
0.75
0.7
0.65
CH4 & CO2 Conversion %
H2/CO
0 2 4 6 8 10 12 14 16 18 20 22 24 26 28
TOS (h)

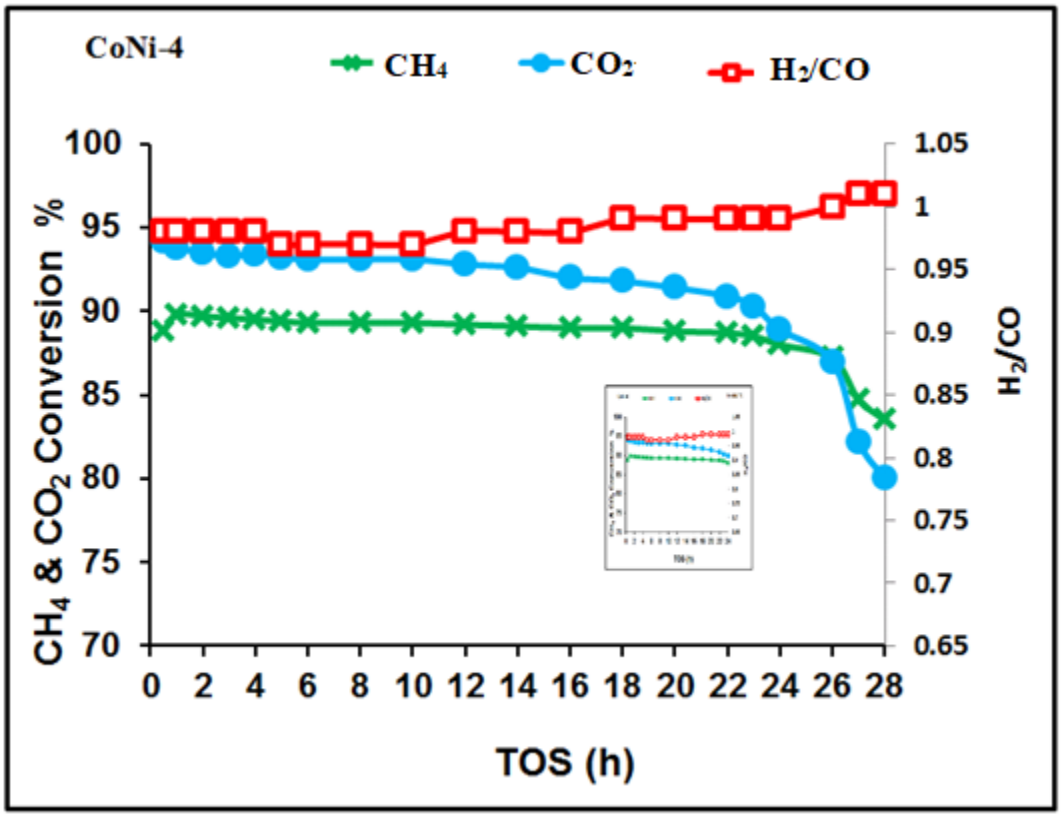
CoNi-4
CH4
CO2
H2/CO
100
95
90
85
80
75
70
1.05
1
0.95
0.9
0.85
0.8
0.75
0.7
0.65
CH4 & CO2 Conversion %
H2/CO
0 2 4 6 8 10 12 14 16 18 20 22 24 26 28
TOS (h)

Fig. 16: long-term stability of CoNi-4 catalyst at 800 °C, atmospheric pressure, CH_4/CO_2 = 1:1. Catalyst was reduced in H_2 at 800 °C, catalyst weight = 150 mg, WHSV = 18000 $ml \cdot g^{-1} \cdot h^{-1}$.

The addition of steam or oxygen to the feed thermodynamically suppresses the coke formation [51]. An increase of the methane conversion with steam addition has been reported in literature [52-54]. Moreover, steam acts as an oxidant removing carbon species from the surface of the catalyst [55]. It is well known that in the presence of a small amount of steam a higher stability of DRM catalysts and a H_2/CO ratio close to unity are obtainable due to the WGS side reaction [53, 54]. In the present study, addition of small amounts of steam or oxygen to the feed has been tested as a way to increase the stability of the CoNi-4 catalyst. The resulting course of CH_4 conversion for CO_2 reforming of methane at 700 °C is compared to conventional DRM in Figure 17. This particular catalyst lost around 9.4% of initial activity in DRM, but only 5.4% in presence of water and only 3.2% in presence of O_2.

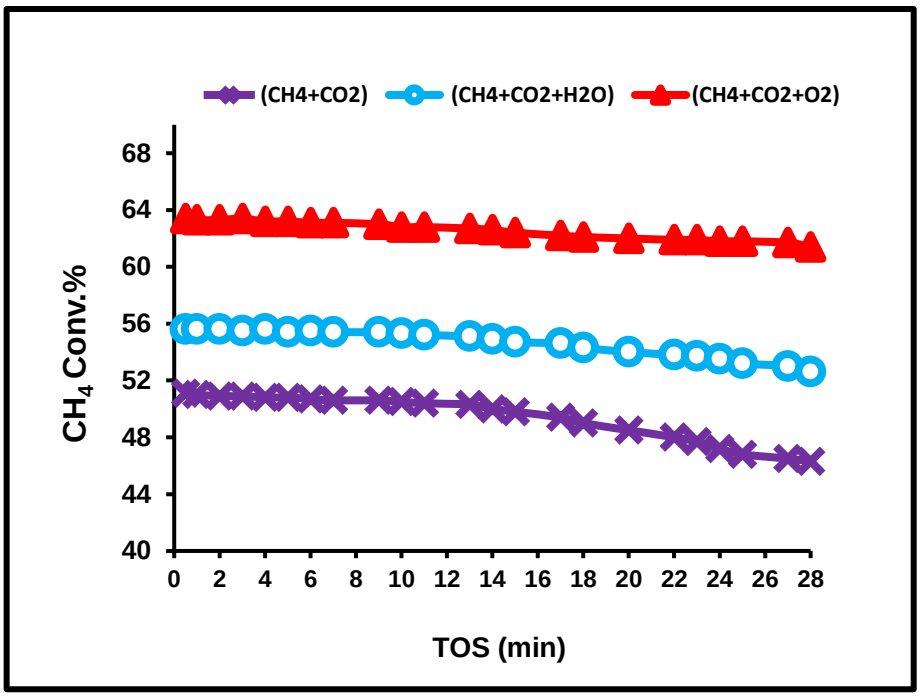

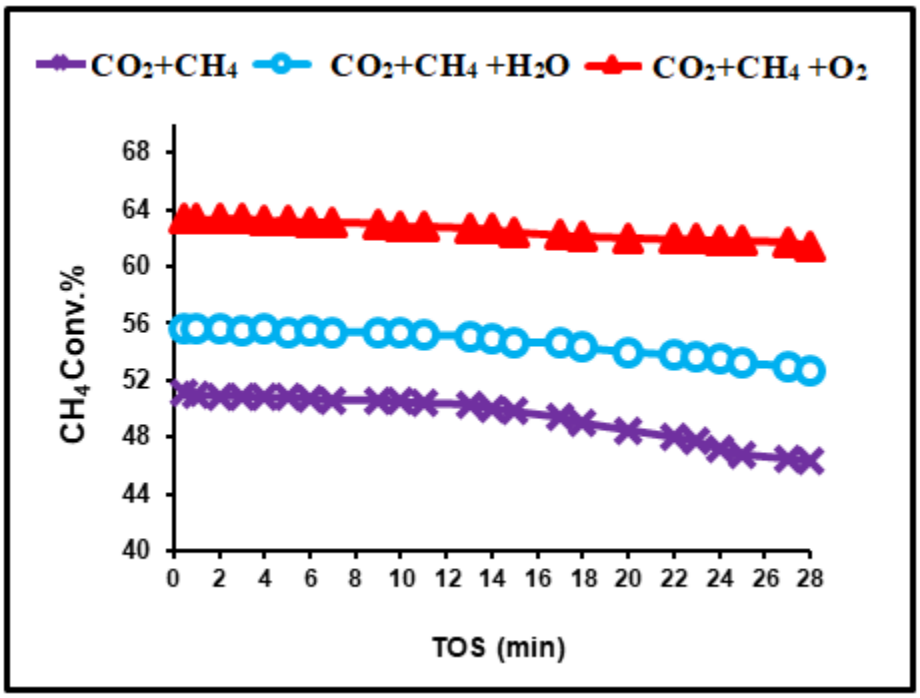

Fig. 17: Effect of steam or oxygen addition on long-term stability of CoNi-4 catalyst at 700 °C, atmospheric pressure, catalyst was reduced in H_2 at 800 °C, catalyst weight = 100 mg.

TGA of spent CoNi-4 catalyst was conducted afterwards (Figure 18). The amount of carbon deposits decreased with the addition of a small amount of water or oxygen, which is in agreement with the catalyst stability (Figure 17).

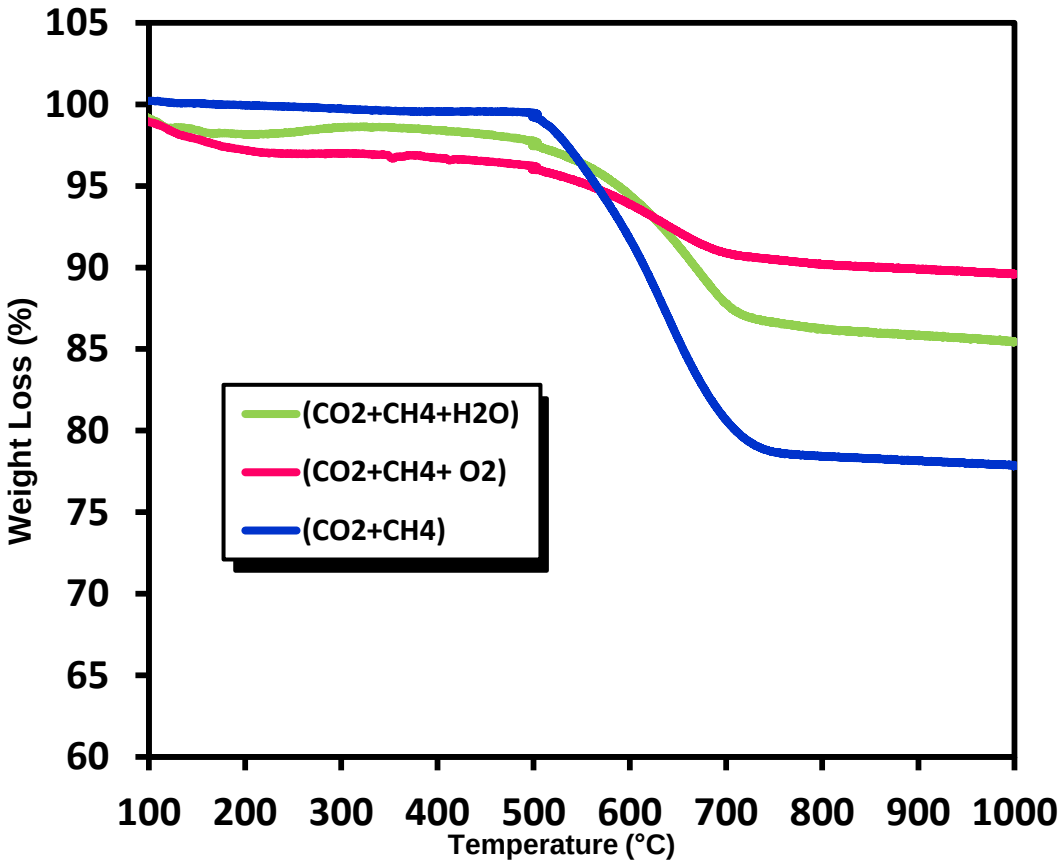

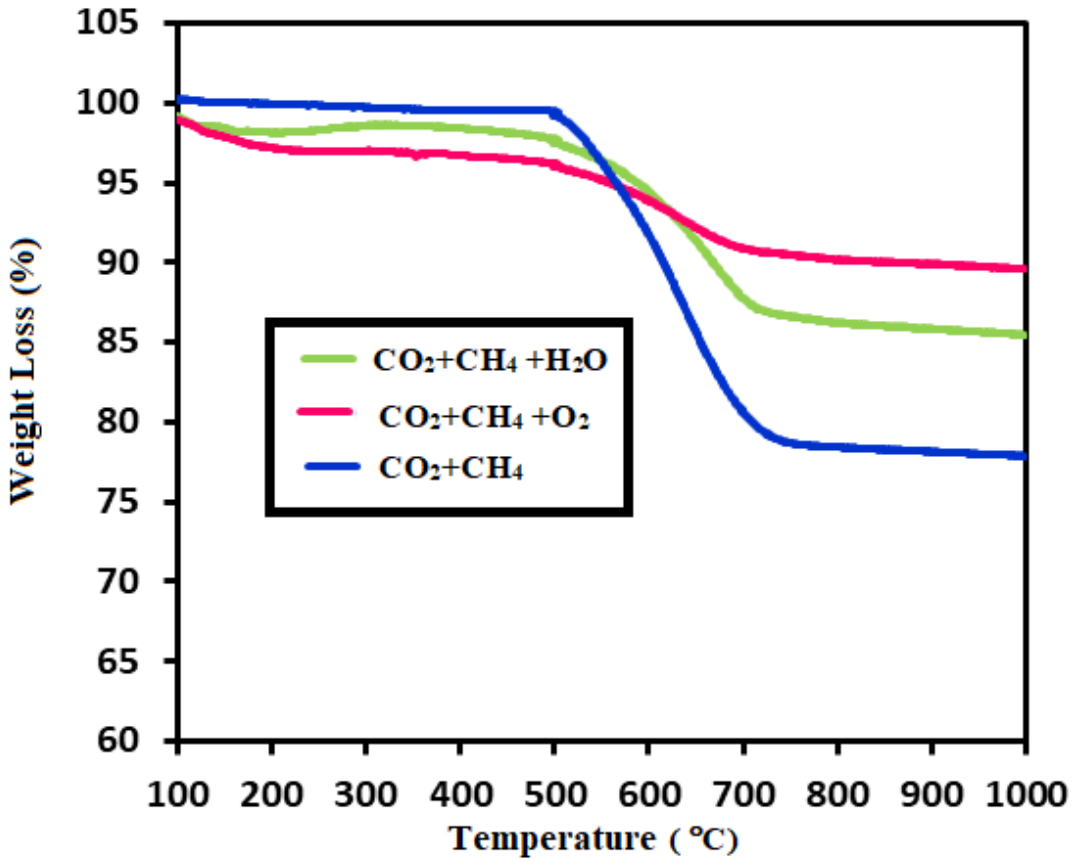

Fig. 18: TGA curves for spent CoNi-4 catalysts used with different feeds at 700°C, measured in N_2 atmosphere with heating rate of 20 K/min.

Conclusions

Various monometallic and bimetallic catalysts supported on Al_2O_3-ZrO_2 (Co, Ni and bimetallic Co-Ni) at different calcination and pre-treatment temperatures were tested for dry reforming of methane. The pre-treatment improved the catalytic performance and bimetallic catalysts outperformed the monometallic catalysts mainly due to synergy between both Ni and Co. Interestingly the higher conversions resulted in higher carbon deposition which played significant role in catalyst deactivation. The least carbon deposition was observed on bimetallic CoNi-4 catalyst calcined under air at 800 °C and

operated at 800 °C after 6 h on stream. This means that high calcination temperature triggers sintering and reduction of surface area and thus particle growth which in turn has an impact on the stability of the catalyst. As it has been reported, this catalyst showed high stability at these conditions for 28 h on stream. The deactivation is assigned to carbon deposition and was confirmed by XRD, TEM and TPO data. The catalyst stability was improved when steam or oxygen were added in the feed stream.

Acknowledgment

The authors would like to express their sincere appreciation to the Deanship of Scientific Research at King Saud University for funding this research project (# RG-1435-078).

References

[1] Khani Y, Shariatinia Z and Bahadoran F. High catalytic activity and stability of $ZnLaAlO_4$ supported Ni, Pt and Ru nanocatalysts applied in the dry, steam and combined dry-steam reforming of methane. Chem. Eng. J. 2016;299: 353-366.

[2] Yang H, Xu Z, Fan M, Gupta R, Slimane RB, Bland AE and Wright I, Progress in carbon dioxide separation and capture: A review. J. Environ. Sci. 2008; 20: 14-27.

[3] Sumrunronnasak S, Tantayanon S, Kiatgamolchai S and Sukonket T, Improved hydrogen production from dry reforming reaction using a catalytic packed-bed membrane reactor with Ni-based catalyst and dense PdAgCu alloy membrane. Int. J. Hydrogen Ener. 2016; 41: 2621-2630.

[4] Usman M, Wan Daud WMA and Abbas HF, Dry reforming of methane: Influence of process parameters- A review. Renew. and Sust. Energ. Rev. 2015; 45: 710-744.

[5] Perez-Camacho MN, Abu-Dahrieh J, Goguet A, Sun K and Rooney D, Self-cleaning perovskite type catalysts for the dry reforming of methane. Chin. J. Catal. 2014; 35: 1337-1346.

[6] Perez-Camacho MN, Abu-Dahrieh J, Rooney D and Sun K, Biogas reforming using renewable wind energy and induction heating. Catal. Today 242, Part A: 2015; 129-138.

[7] Charisiou ND, Siakavelas G, Papageridis KN, Baklavaridis A, Tzounis L, Avraam DG and Goula MA, Syngas production via the biogas dry reforming reaction over nickel supported on modified with CeO_2 and/or La_2O_3 alumina catalysts. J. Nat. Gas Sci. Eng. 2016; 31: 164-183.

[8] Niu J, Du X, Ran J and Wang R, Dry (CO_2) reforming of methane over Pt catalysts studied by DFT and kinetic modeling. Appl. Surf. Sci. 2016; 376: 79-90.

[9] Chengyun Z, Cui L, Danlian H, Guangming Z, Chen Z, Min C, Liang H, Jia W, Weiping X, Ming W, Xiaofeng W, Lei Q, Highly porous carbon nitride by supramolecular preassembly of monomers for photocatalytic removal of sulfamethazine under visible light driven. Appl. Catal. B: Environ. 2018; 220: 202-210.

[10] Yang Y, Chen Z, Danlian H, Guangming Z, Jinhui H, Cui L, Chengyun Z, Wenjun W, Hai G, Wenjing X, Rui D, Min C, Weiping X, Boron nitride quantum dots decorated ultrathin porous g-C_3N_4: Intensified exciton dissociation and charge transfer for promoting visible-light-driven molecular oxygen activation. Appl. Catal. B: Environ. 2019; 245: 87-99.

[11] Chengyun Z, Cui L, Chen Z, Guangming Z, Danlian H, Min C, Liang H, Weiping X, Ming C, Jiajia W, Yang Y, Longbo J, Semiconductor/boron nitride composites:

Synthesis, properties, and photocatalysis applications. Appl. Catal. B: Environ. 2018; 238: 6-18.

[12] Chengyun Z, Cui L, Piao X, Guangming Z, Danlian H, Zhihao L, Chen Z, Min C, Liang H, Jia W, Fei C, Weiping X, Rui D, Rational Design of Carbon-Doped Carbon Nitride/$Bi_{12}O_{17}Cl_2$ Composites: A Promising Candidate Photocatalyst for Boosting Visible-Light-Driven Photocatalytic Degradation of Tetracycline. ACS Sustain. Chem. Eng. 2018; 6: 6941-6949.

[13] Xiang R, Ruixiang G, Yong Z, Danni L, Dan W, Xu S, Bin D, Qin W, Cobalt–borate nanowire array as a high-performance catalyst for oxygen evolution reaction in near-neutral media. J. Mater. Chem. A 2017; 5: 7291-7294.

[14] Xiang R, Dan W, Ruixiang G, Xu S, Hongmin M, Tao Y, Yong Z, Bin D, Qin W, Liang C, Self-supported $CoMoS_4$ nanosheet array as an efficient catalyst for hydrogen evolution reaction at neutral pH. Nano Res. 2018; 11: 2024-2033.

[15] Xiang R, Xuqiang J, Yicheng W, Dan W, Yong Z, Min M, Zhiang L, Abdullah MA, Qin W, Xuping S, In situ electrochemical development of copper oxide nanocatalysts within a TCNQ nanowire array: a highly conductive electrocatalyst for the oxygen evolution reaction. Chem. Comm. 2018; 54: 1425-1428.

[16] Jinxiu Z, Xiang R, Qingzhi H, Dawei F, Xu S, Xuan K, Qin W, Dan W, Ultra-thin wrinkled NiOOH–$NiCr_2O_4$ nanosheets on Ni foam: an advanced catalytic electrode for oxygen evolution reaction. Chem. Comm. 2018; 54: 4987-4990.

[17] Jinxiu Z, Xiang R, Hongmin M, Xu S, Yong Z, Tao Y, Qin W, Dan W, Synthesis of Self-Supported Amorphous $CoMoO_4$ Nanowire Array for Highly Efficient Hydrogen Evolution Reaction. ACS Sustain. Chem. Eng. 2017; 5: 10093-10098.

[18] Benrabaa R, Lofberg A, Rubbens A, Bordes-Richard E, Vannier RN and Barama A, Structure, reactivity and catalytic properties of nanoparticles of nickel ferrite in the dry reforming of methane. Catal. Today 2013; 203: 188-195.

[19] Hao Z, Zhu Q, Jiang Z, Hou B and Li H, Characterization of aerogel Ni/Al_2O_3 catalysts and investigation on their stability for CH4-CO2 reforming in a fluidized bed. Fuel Process Technol. 2009; 90: 113-121.

[20] Luengnaruemitchai A and Kaengsilalai A, Activity of different zeolite-supported Ni catalysts for methane reforming with carbon dioxide. Chem. Eng. J. 2008; 144: 96-102.

[21] Pompeo F, Nichio NN, Gonzalez MG and Montes M, Characterization of Ni/SiO_2 and $Ni/Li\text{-}SiO_2$ catalysts for methane dry reforming. Catal. Today 2005; 107-108: 856-862.

[22] Fakeeha AH, Khan WU, Al-Fatesh AS and Abasaeed AE, Stabilities of zeolite-supported Ni catalysts for dry reforming of methane. Chin. J. Catal. 2013; 34: 764-768.

[23] Xiang X, Zhao H, Yang J, Zhao J, Yan L, Song H and Chou L, Nickel based mesoporous silica-ceria-zirconia composite for carbon dioxide reforming of methane. Appl. Catal. A: G 2016; 520: 140-150.

[24] Albarazi A, Galvez ME and Da Costa P, Synthesis strategies of ceria-zirconia doped Ni/SBA-15 catalysts for methane dry reforming. Catal. Comm. 2015; 59: 108-112.

[25] Wolfbeisser A, Sophiphun O, Bernardi J, Wittayakun J, Fottinger K and Rupprechter G, Methane dry reforming over ceria-zirconia supported Ni catalysts. Catal. Today in press 2016; 277: 234-245.

[26] Rahemi N, Haghighi M, Babaluo AA, Jafari MF and Estifaee P, Synthesis and physicochemical characterizations of $Ni/Al_2O_3\text{-}ZrO_2$ nanocatalyst prepared via

impregnation method and treated with non-thermal plasma for CO_2 reforming of CH_4. J. Ind. Eng. Chem. 2013; 19: 1566-1576.

[27] Bellido JDA, De Souza JE, MPeko J-C and Assaf EM, Effect of adding CaO to ZrO_2 support on nickel catalyst activity in dry reforming of methane. Appl. Catal. A: G 2009; 358: 215-223.

[28] Al-Fatesh ASA and Fakeeha AH, Effects of calcination and activation temperature on dry reforming catalysts. J. S. Chem. Soc. 2012; 16: 55-61.

[29] Rezgui Y and Guemini M, Effect of pretreatment conditions on the catalytic performance of Ni-Pt-W supported on amorphous silica-alumina catalysts: Part 1. Catalysts prepared by a sol-gel method. Appl. Catal. A: General 335: 103-111 (2008).

[30] Chen L, Lu Y, Hong Q, Lin J and Dautzenberg FM, Catalytic partial oxidation of methane to syngas over Ca-decorated-Al_2O_3-supported Ni and NiB catalysts. Appl. Catal. A: G 2005; 292: 295-304.

[31] Wang HY and Ruckenstein E, Conversions of Methane to Synthesis Gas over Co/γ-Al_2O_3 by CO_2 and/or O_2. Catal. Lett. 2001; 75: 13-18.

[32] Sun H, Wang H and Zhang J, Preparation and characterization of nickel-titanium composite xerogel catalyst for CO_2 reforming of CH_4. Appl. Catal. B: Environ. 2007; 73: 158-165.

[33] Al-Fatesh A, Suppression of carbon formation in CH4-CO2 reforming by addition of Sr into bimetallic Ni-Co/γ-Al_2O_3 catalyst. J. K. S. U. – Eng. Sci. 2015; 27: 101-107.

[34] Guo C, Hu P, Yu L and Yuan F, Synthesis and characterization of ZrO_2 hollow spheres. Mater. Lett. 2009; 63: 1013-1015.

[35] Kruglova MA and Yaroshenko MP, Preparation and characteristics of zirconium-aluminum oxide system. Russ J. Appl. Chem. 2007; 80: 1461-1467.

[36]. Zhang, J.; Wang, H.; Dalai, A. K. Development of stable bimetallic catalysts for carbon dioxide reforming of methane J. Catal. 2007, 249: 300-310.

[37] Osaki T and Mori T, Kinetic studies of CO_2 dissociation on supported Ni catalysts. React Kinet Catal. Lett. 2005; 87: 149-156.

[38] Zhu Z-Z, Wang Z and Li H-L, Functional multi-walled carbon nanotube/polyaniline composite films as supports of platinum for formic acid electrooxidation. Appl. Surf. Sci. 2008; 254: 2934-2940.

[39] Lu C, Su F and Hu S, Surface modification of carbon nanotubes for enhancing BTEX adsorption from aqueous solutions. Appl. Surf. Sci. 2008; 254: 7035-7041.

[40] Li ZQ, Lu CJ, Xia ZP, Zhou Y and Luo Z, X-ray diffraction patterns of graphite and turbostratic carbon. Carbon 2007; 45: 1686-1695.

[41] Singh KSW, Rouquerol J, Bergeret G, Gallezot P, Vaarkamp M, Koningsberger DC, Datye AK, Niemantsverdriet JW, Butz T, Engelhardt G, Mestl G, Knözinger H and Jobic H, Characterization of Solid Catalysts: Sections 3.1.1 – 3.1.3, in Handbook of Heterogeneous Catalysis. Wiley-VCH Verlag GmbH, pp. 427-582 2008.

[42] Matthew M. Yung, Erik M. Holmgreen, Umit S. Ozkan, Cobalt-based catalysts supported on titania and zirconia for the oxidation of nitric oxide to nitrogen dioxide. J. Catal. 2007; 247: 356–367.

[43] Al-Fatish ASA, Ibrahim AA, Fakeeha AH, Soliman MA, Siddiqui MRH and Abasaeed AE, Coke formation during CO_2 reforming of CH4 over alumina-supported nickel catalysts. Appl. Catal. A: G 2009; 364: 150-155.

[44] Gonzalez-delaCruz VM, Pereniguez R, Ternero F, Holgado JP and Caballero A, In Situ XAS Study of Synergic Effects on Ni-Co/ZrO_2 Methane Reforming Catalysts. J. Phys. Chem. C 116: 2012; 2919-2926.

[45] Zhang J, Wang H and Dalai AK, Effects of metal content on activity and stability of Ni-Co bimetallic catalysts for CO_2 reforming of CH4. Appl. Catal. A: G 2008; 339: 121-129.

[46] Arkatova LA, The deposition of coke during carbon dioxide reforming of methane over intermetallides. Catal. Today 2010; 157: 170-176.

[47] Kim JH, Suh DJ, Park TJ and Kim KL, Effect of metal particle size on coking during CO_2 reforming of CH_4 over Ni-alumina aerogel catalysts. Appl. Catal. A: G 2000; 197: 191-200.

[48] Xu Z, Li Y, Zhang J, Chang L, Zhou R and Duan Z, Bound-state Ni species - a superior form in Ni-based catalyst for CH_4/CO_2 reforming. Appl. Catal. A: G 2001; 210: 45-53.

[49] Kitiyanan B, Alvarez WE, Harwell JH and Resasco DE, Controlled production of single-wall carbon nanotubes by catalytic decomposition of CO on bimetallic Co-Mo catalysts. Chem Phys Lett. 2000; 317: 497-503.hju

[50] Osaki T and Mori T, Kinetics of the reverse-Boudouard reaction over supported nickel catalysts. React. Kinet. Catal. Lett. 2006; 89: 333-339.

[51] Wang W, Su C, Wu Y, Ran R and Shao Z, Progress in Solid Oxide Fuel Cells with Nickel-Based Anodes Operating on Methane and Related Fuels. Chem. Rev. 2013; 113: 8104-8151.

[52] Soria MA, Mateos-Pedrero C, Guerrero-Ruiz A and Rodriguez-Ramos I, Thermodynamic and experimental study of combined dry and steam reforming of methane on Ru/ ZrO_2-La_2O_3 catalyst at low temperature. Int. J. Hydrogen Ener. 2011; 36: 15212-15220.

[53] O–zkara-Aydinoglu S, Thermodynamic equilibrium analysis of combined carbon dioxide reforming with steam reforming of methane to synthesis gas. Int. J. Hydrogen Ener. 2010; 35: 12821-12828.

[54] O–zkara-Aydinoglu S and Aksoylu AE, CO_2 reforming of methane over Pt-Ni/Al_2O_3 catalysts: Effects of catalyst composition, and water and oxygen addition to the feed. Int. J. Hydrogen Ener. 2011; 36: 2950-2959.

[55] Eltejaei H, Reza Bozorgzadeh H, Towfighi J, Reza Omidkhah M, Rezaei M, Zanganeh R, Zamaniyan A and Zarrin Ghalam A, Methane dry reforming on Ni/$Ce_{0.75}Zr_{0.25}O_2$–$MgAl_2O_4$ and Ni/$Ce_{0.75}Zr_{0.25}O_2$–γ-alumina: Effects of support composition and water addition. Int. J. Hydrogen Ener. 2011; 37: 4107-4118.